Research Square

Preprints are preliminary reports that have not undergone peer review.
They should not be considered conclusive, used to inform clinical practice,
or referenced by the media as validated information.

The analysis of genetic variants in nine patients with Nemaline Myopathy: Implications for diagnosis and genetic counseling

Bingbo Zhou
State Key Laboratory of Digital Medical Engineering, School of Biological Science and Medical Engineering, Southeast University
Chuan Zhang
The Center of Medicine Genetic in Gansu Provincial Maternity and Child-care Hospital
Xiaojuan Lin
The Center of Prenatal Diagnostic in Gansu Provincial Maternity and Child-care Hospital
Panpan Ma
The Center of Medicine Genetic in Gansu Provincial Maternity and Child-care Hospital
Yupei Wang
The Center of Medicine Genetic in Gansu Provincial Maternity and Child-care Hospital
Lei Zheng
The Center of Medicine Genetic in Gansu Provincial Maternity and Child-care Hospital
Shengju Hao
The Center of Medicine Genetic in Gansu Provincial Maternity and Child-care Hospital
Ling Hui
The Center of Medicine Genetic in Gansu Provincial Maternity and Child-care Hospital
Yunfei Bai
whitecf@seu.edu.cn

State Key Laboratory of Digital Medical Engineering, School of Biological Science and Medical Engineering, Southeast University

Article

Keywords: Nemaline myopathy, Whole-exome sequencing, NMA, AlphaFold3, NEB, Coarse-grained

Posted Date: July 20th, 2026

DOI: https://doi.org/10.21203/rs.3.rs-10104013/v1

License: This work is licensed under a Creative Commons Attribution 4.0 International License. Read Full License

Additional Declarations: No competing interests reported.

Version of Record: A version of this preprint was published at Scientific Reports on October 15th, 2026. See the published version at https://doi.org/10.1038/s41598-026-74441-3.

Abstract

Nemaline myopathy (NM) is a rare and hereditary myopathy caused by several related genes have been identified, thus exhibiting significant clinical and genetic heterogeneity. This study retrospectively analyzed 9 patients with NM. We utilized WES testing and bioinformatics analysis were performed on 9 families. Normal Mode Analysis (NMA) was used to evaluate the impact of missense variants in the *NEB* gene on the thermodynamic stability of the nebulin protein. The WES results revealed 17 variants in the *TPM3*, *NEB*, and *ACTA1* genes in the 9 patients. According to the variant classification criteria published by the American College of Medical Genetics and Genomics (ACMG), approximately two-thirds of the variants were classified as pathogenic or likely pathogenic, while the remaining variants were classified as of uncertain significance. Meanwhile, our coarse-grained network meta-analysis of missense variants in the *NEB* gene shown that, compared with the other two missense variants, the c.9146T > G (p. Ile3049Ser) variant exhibited a significantly higher entropy value within the protein's thermodynamic range, which may lead to protein instability. This study provides valuable insights and approaches for the diagnosis, prognosis, and genetic counseling of NM. By reviewing these cases, we hope to enrich the existing NM knowledge base.

1. Introduction

Nemaline myopathy (NM) is a muscle disorder characterized by a wide spectrum of clinical severity. Its primary etiology lies in abnormalities of muscle fibers caused by genetic mutations, resulting in a disease syndrome predominantly characterized by muscle weakness. Patients may also present with symptoms such as muscle atrophy, delayed motor development, muscle fatigability, myalgia, muscle cramps, and respiratory dysfunction[1]. According to studies conducted in Finland, the estimated annual incidence of this disease is approximately 1 in every 50,000 live births; however, the incidence is relatively higher within the Amish community[2]. NM exhibits high genetic heterogeneity, and a total of 12 genes have been definitively identified (corresponding to subtypes NEM1–NEM12), namely *TPM3*[3], *NEB*[4], *ACTA1*[5], *TPM2*[6], *TNNT1*[7], *KBTBD13*[8], *CFL2*[9], *KLHL40*[10], *KLHL41*[11], *LMOD3*[12], *MYPN*[13], and *TNNT3*[14]. Most of these genes encode components of the thin filaments within skeletal muscle sarcomeres. Since skeletal muscle sarcomeres are primarily composed of thick filaments (formed by myosin) and thin filaments (formed by actin), defects in the genes encoding these components lead to functional impairment of the skeletal muscle sarcomere, thereby resulting in muscle weakness.

Nemaline myopathy type 2 (NEM2) is a skeletal muscle disorder characterized by an autosomal recessive mode of inheritance, and its primary etiology lies in defects within the *NEB*[4]. A recent study identified biallelic pathogenic variants in the *NEB* in 24 individuals. All of these patients presented with symptoms of muscle weakness and atrophy, and muscle biopsies subsequently confirmed the presence of nemaline rods within their muscle tissue[4, 15]. Gajda reported a case involving a child who, during infancy, presented with generalized hypotonia, muscle weakness, and delayed motor development; the child did not begin practicing walking—even with the aid of orthotic braces—until the age of two. Furthermore, this patient exhibited diminished deep tendon reflexes and suffered from recurrent respiratory tract infections[16]. These studies demonstrate that *NEB* deficiency is clinically heterogeneous, and its manifestations extend beyond mere muscle weakness and atrophy to encompass the various clinical symptoms described above. In summary, the most common clinical presentation is early-onset or congenital muscle weakness, primarily affecting the proximal limb muscles.

Within the field of neuromuscular disorders, it is noteworthy that NEM2 is a condition that is easily overlooked. Although it is an extremely rare disease, gaining a comprehensive understanding of it is of paramount importance. Grasping the theoretical underpinnings of this disorder facilitates early diagnosis and treatment, thereby holding the potential to improve patient outcomes. In the present study, we provide a detailed account of nine patients with NM, and by meticulously documenting and presenting each individual case, we aim to contribute to the medical community's understanding of this disease. This endeavor is expected to provide a more precise basis for the diagnosis of future cases, as well as offer critical references and insights for the development of targeted therapeutic interventions.

2. Materials and Methods

2.1 Sample collection and DNA extraction

In this study, a total of 9 patients were enrolled based on genotype from January 2018 to December 2024. Nearly a thousand WES tests were performed on patients suspected of having neuromuscular diseases in our department, and 9 patients (1.02%) were diagnosed with nemaline myopathy based on the high correlation between the clinical phenotype and genotype. Each patient and(or) their family members have been informed and signed a written informed consent form, and this study was approved by the Institutional Review Boards of Gansu Provincial Maternity and Child-care Hospital. We have meticulously collected detailed clinical phenotypes and the corresponding relevant laboratory test indicators of these patients. Peripheral blood samples from patients and their family members were collected into 5mL tubes and anticoagulated with EDTA. Fetal amniotic fluid samples were obtained under aseptic conditions. Subsequently, 15 mL of the amniotic fluid was centrifuged, after which the supernatant was removed, and the precipitation was frozen and set aside for future research. DNA was then extracted via the magnetic bead method, and its concentration was measured via Nanodrop 2000 to ensure it met the experimental standards (The ratio of OD260 to OD280 is between 1.8 and 2.0).

2.2 Trio-WES and Bioinformatics analysis

Genomic DNA was extracted from peripheral blood or frozen muscle of the patients. Exon capture was performed using MGI Easy Exome Capture V4 Probe Kit. The MGISEQ-2000 series sequencer was employed for sequencing, attaining a target sequencing rate of at least 99% and an average depth exceeding 200×. The sequenced raw data was processed with Fastp to eliminate aptamers and low-quality reads. Paired-end reads were aligned to the reference genome by using BWA. Base quality scores were recalibrated with GATK, and variants such as SNPs and indels were identified based on sequence depth and quality. The proband's phenotype information originated from hospital charts and was verified by the Human Phenotype Ontology database. To guarantee the accuracy and reliability of the sequencing results, strict quality control measures were adopted. The extracted DNA was meticulously inspected for quality

and contaminants. The sequencing process was controlled to achieve optimal sequencer performance. After sequencing, advanced algorithms and software analyzed and interpreted the data to identify significant variants, which were subsequently validated and characterized. The database assisted in confirming and refining the phenotype information. The final likely variant sites were validated once again by Sanger sequencing.

2.3 Sanger sequencing

In this study, the Sanger sequencing method was utilized to analyze the suspected gene fragments. Taking the extracted genomic DNA as a template, a sequencing system was prepared, which consisted of template DNA, sequencing primers, and the Big Dye Terminator reaction mix. Following cyclic sequencing reactions and purification via ethanol/sodium acetate precipitation, capillary electrophoresis separation and fluorescence signal detection were conducted using an ABI 3500Dx DNA analyzer. The final stage of the process entailed the recognition of the base sequence, the alignment of this sequence, and the detection of variants. These were accomplished through the use of such software as Sequencing Analysis and SnapGene (from GSL Biotech; available at www.snapgene.com).

2.4 Protein structure prediction and NMA

Due to limitations regarding sequence length in the online version of AlphaFold3 (capped at 5,000 amino acids), it was not possible to directly compute the structure of full-length Nebulin (8,525 amino acids). Consequently, we divided the wild-type Nebulin into two segments based on its super-repeat sequences —WT-1 and WT-2—for structural prediction, and the resulting data were subsequently merged to enable visualization of the complete structure. For the mutant proteins, predictions were conducted using two distinct approaches based on the type of variant: the nonsense mutations, which result in truncated proteins of fewer than 5,000 amino acids, were predicted directly. Conversely, the two frameshift mutations were predicted based on a region spanning 2,000 amino acids upstream and downstream of the mutation site (a range of ± 2,000 residues), specifically encompassing the C-terminal SH3 domain (residues 4,525–8,525).

Meanwhile, we compared the energetic effect of the three missense variants (p. Arg6177His, p. Leu6267Pro, and p. Ile3049Ser) on nebulin and searched the HGMD for other cases of NEM2 due to missense variants. We evaluated the impact of missense variants on protein stability via the utilization of coarse-grained NMA. NMA was integrated within the Bio3d package[17], which offers multiple Efficient Elastic Network Model (ENM) force fields. For each variant, we subtracted the WT complex entropy from the missense variant entropy and normalized the difference (ΔG) to the maxi-mum absolute values. Cluster analysis was performed using R software.

For each ΔG curve, we established an interval R, defined as [mean(ΔG) − 0.5 × std(ΔG), mean(ΔG) + 0.5 × std(ΔG)]. Within this framework, we derived 6 key parameters: G1 is defined as the absolute mean of ΔG values falling outside interval R, serving to quantify significant energy fluctuations that deviate from the central tendency; G2 is defined as the absolute mean of ΔG values falling within interval R, reflecting baseline fluctuations during a steady state; and G3 is defined as the coefficient of variation (std(ΔG)/mean(ΔG)), used to measure relative variability. Furthermore, we defined G4 as the maximum absolute ΔG value outside interval R, representing the most intense direct perturbation induced by a mutation; G5 as the maximum absolute ΔG value within interval R, capturing the upper bound of baseline fluctuations; and G6 as a composite metric (G3 × [1 + |G1 - G2|/(G1 + G2)]), which integrates relative variability (G3) with the disparity between extreme fluctuations (G1) and baseline fluctuations (G2).

Compared to the wild type (WT), the entropy profiles of the various variants encompass the following aspects: I. Overall relative stability (mean ΔG). II. Fluctuation range (standard deviation of ΔG). III. Local perturbation intensity (G4). IV. Baseline structural flexibility (G5). V. Comprehensive stability-fluctuation index (G6). This multiparametric analytical approach enables a comprehensive characterization of mutational effects, distinguishing between direct perturbations proximal to the mutation site (G4) and distal allosteric effects (G5), while S6 provides a holistic measure of thermodynamic resilience.

3. Results

3.1 Clinical features

This case series encompasses patients spanning a wide age range, ranging from a fetus at 25 + 5 weeks of gestation to 14-year-old adolescents, with a balanced ratio of 1:1 maintained between male and female patients (Fig. 1, Table 2 and Table S1). When contemplating the typical clinical symptoms, developmental and growth delays emerge as a matter of particular concern, which was exemplified by patients 1, 2, 4, 5 and 7. We have identified multiple heart diseases in patients 1, 4, and 8, including ventricular septal defects (VSD), patent foramen ovale (PFO), right heart enlargement, and pulmonary arterial hypertension, indicating that cardiovascular disease is also of significant concern in NM patients. Additionally, we discovered recurrent respiratory problems in patients 2, 4, 6, and 8, suggesting that gene mutations also severely impact the function of respiratory muscles in NM patients, leading to relapsing pneumonia and relapsing bronchopneumonia. The extensive array of complex disorders in these individuals necessitates comprehensive and individualized medical care and treatment plans. The variations in age, sex, and specific symptoms emphasize the complexity and challenges involved in diagnosing and treating these conditions. To offer these patients the best possible care and enhance their prognosis, further research and tailored strategies are indispensable.

3.2 Genetics findings

We discovered a total of seventeen variants in these probands from nine unrelated families through Whole-exome sequencing technology. Specifically, this included seven splice variants which accounted for 41.2% of the total variants, five missense variants which constituted 29.4% of the total variants, three frameshift variants which made up 17.6% of the total variants, and two nonsense variants which represented 11.8% of the total variants. According to the ACMG guidelines, sex variants (35.3%) were classified as Pathogenic, sex variants (35.3%) were classified as Likely pathogenic, and the remaining five

variants (29.4%) were classified as Uncertain significance (Table 1). The *TPM3* and *ACTA1* were both denovo variants, whereas the *NEB* is inherited from both parents.

3.3 Variants in *NEB*

The result revealed that the compound heterozygous variants in six and a homozygous variant in one of the nine NM patients within the *NEB* gene. In patient 1, the heterozygous splicing variant c.4720-1G > A was inherited from the father, and the heterozygous missense variant c.18530G > A was inherited from the mother (Table 1 and Figure S1). In patient 2, the variants c.18800T > C and c.16909-3_16911delCAGCCA were inherited from the mother, while the variants c.11182-8T > A and c.7897dupT were inherited from the father (Table 1 and Figure S2). However, the loss-of-function (LOF) variants c.16909-3_16911delCAGCCA and c.7897dupT constitute compound heterozygous variants and have been classified as likely pathogenic. Accordingly, we hypothesize that it is precisely these compound heterozygous variants that underlie the etiology of NEM2 in this patient. This situation indicates that, although the clinical significance of variants c.11182-8T > A and c.18800T > C remains unclear, further research may be required to precisely elucidate whether they exert a synergistic effect with the two LOF variants. In patient 3, the heterozygous splicing variant c.21417 + 3A > G was inherited from the mother, and c.9103-4_9103-3delTT was inherited from the father (Table 1 and Figure S3). In patient 4, the variant c.24177_24178delAG was inherited from the father (Table 1 and Fig. 2C), and the variant c.23638delC was inherited from the mother (Table 1 and Fig. 2C). In patient 5, the variant c.7727G > A was inherited from the father, and the heterozygous splicing variant c.21417 + 3A > G was inherited from the mother (Table 1 and Figure S5). In patient 6, the heterozygous nonsense variant c.412C > T was inherited from the father, and the heterozygous missense variant c.9146T > G was inherited from the mother (Table 1 and Figure S6). In patient 9, the homozygous splicing variant c.21417 + 3A > G were inherited from the parents (Table 1 and Figure S9). These 15 variants were all located in the protein repeat region (Fig. 2A).

3.4 Variants in *TPM3*

We identified a heterozygous variant in one of the nine NM patients within the *TPM3* gene. In patient 7, the denovo variant c.502C > T located in exon 5, the parents are wild type. We also collected the previously reported variants of the *TPM3* gene for visualization (Fig. 3A). The results showed that the variant c.502C > T might also be a hotspot mutation in NEM1, which have appeared a total of five times at the same position in the protein including in this study (Table 1 and Figure S7). To predict whether the missense variant would induce protein structural instability and thereby assess its pathogenicity, we utilized DynaMut2[18] which was designed to evaluate the alterations in stability and flexibility resulting from *TPM3* gene missense mutations (Fig. 3B). The predicted stability change ($\Delta\Delta^{Stability}$) of the tropomyosin alpha-3 chain protein was 0.08 kcal/mol. This numerical value implies that the mutation may confer greater stability to the protein, and we inferred that this mutation likely does not play a pivot-al regulatory role in muscle contraction.

3.5 Variants in *ACTA1*

We identified a denovo heterozygous variants in one of the nine NM patients within the *ACTA1* gene. In patient 8, the variant c.400A > G located in exon 3, the parents are wild type. We also collected the previously reported variants of the *ACTA1* gene for visualization (Fig. 3C). The results showed that the variant c.400A > G might also be a hotspot mutation in NEM3, which have appeared a total of four times at the same position in the protein including in this study (Table 1 and Figure S8). We assessed the impact of mutations on actin protein dynamics and stability resulting from vibrational entropy changes (Fig. 3D). The predicted ΔΔStability of the actin protein was − 0.29 kcal/mol and suggested that the mutation renders the protein highly unstable. Actin protein, being the primary component of the thin filaments in striated muscle myofibrils, intertwines with tropomyosin and troponin to form the myofibril thin filaments in muscles. Given that the mutation induces extreme protein instability, it was likely to have a severe impact on muscle contraction.

3.6 Structural prediction of mutant proteins

The protein encoded by the *NEB* gene is termed Nebulin, which is a large protein component of the cytoskeleton matrix and coexists with thick and thin filaments in skeletal muscle segments. To identify the whole structure of the Nebulin protein and the structure of mutant protein, we used AlphaFold3 for accurate prediction based on the presence or absence of these super-repeat sequences (Fig. 2B and 2C). Simultaneously, we conducted a preliminary exploration of the alterations in the protein structure that occur before and after *ACTA1* mutation (Fig. 3C), and the random seed was set to 256.

3.7 *NEB* missense variants alter protein stability

NEM2 is predominantly attributed to LOF variants in the *NEB* gene. Nevertheless, Patient 1, Patient 2, and Patient 6 harbored missense variants, namely p. Arg6177His, p. Leu6267Pro, and p. Ile3049Ser respectively. To elucidate whether these missense variants influence protein stability, we analyzed the mutant and wild-type proteins using coarse-grained NMA. The results indicated that the p. Ile3049Ser variant directly disrupted protein stability, while the p. Arg6177His and p. Leu6267Pro variants had a relatively lower capacity to directly disrupt protein stability (Fig. 4 and Figure S10). This finding is a crucial determinant in explaining the difference symptoms presented by Patient 1 and Patient 6. Furthermore, we conducted an analysis of coarse-grained NMA for likely pathogenic missense variants listed in the Clinvar and HGMD databases. The analysis revealed that the missense variant p. S6366I (p. Ser6366Ile) induced significant and extreme energetic perturbations, potentially disrupting crucial structures or functions. In contrast, the missense variant p. D498G (p. Asp498Gly) demonstrated extremely low energetic perturbations (Fig. 4B).

Table 1
Genetic information of patients with NM

Patient	Gene (Transcript Accession)	genomics pos (GRCh37/Hg19)	c. HGVS (p. HGVS)	Exon or Intron	Mutation type (Zygosity)	Clinical significance	ACMG Classification Criteria
1	*NEB* (*NM_001164508.2*)	chr2:152522916	c.4720-1G > A (p.?)	IVS40	Canonical-Splicing (Het)	LP	PVS1+PM2_Supporting
		chr2:152420386	c.18530G > A (p. Arg6177His)	EX118	Missense (Het)	VUS	PM3+ PM2_Supporting+PP3
2	*NEB* (*NM_001164508.2*)	chr2:152419216	c.18800T > C (p. Leu6267Pro)	EX120	Missense (Het)	VUS	PM2_Supporting+PM3
		chr2:152432311–152432316	c.16909-3_16911delCAGCCA (p.?)	EX107	Splicing (Het)	LP	PVS1+PM2_Supporting
		chr2:152472631	c.11182-8T > A (p.?)	IVS75	Splicing (Het)	VUS	PM2_Supporting+PM3
		chr2:152500390–152500390	c.7897dupT (p. Cys2633Leufs*16)	EX57	Frameshift (Het)	LP	PVS1+PM2_Supporting
3	*NEB* (*NM_001164508.2*)	chr2:152389953	c.21417 + 3A > G (p.?)	IVS144	Splicing (Het)	P	PM4+PM3_Very Strong+PM2_Supp
		chr2:152490481–152490483	c.9103-4_9103-3delTT (p.?)	IVS64	Splicing (Het)	VUS	PM2_Supporting+PM3
4	*NEB* (*NM_001164508.2*)	chr2:152354807–152354808	c.24177_24178delAG (p. Arg8059Serfs*9)	EX171	Frameshift (Het)	P	PVS1+PM2_Supporting+PM3_Supp
		chr2:152362692	c.23638delC (p. His7880Thrfs*5)	EX165	Frameshift (Het)	P	PVS1+PM2_Supporting+PM3
5	*NEB* (*NM_001164508.2*)	chr2:152500561	c.7727G > A (p. Trp2576Ter)	EX57	Nonsense (Het)	P	PVS1+PM2_Supporting+PM3
		chr2:152389953	c.21417 + 3A > G (p.?)	IVS144	Splicing (Het)	P	PM4+PM3_Very Strong+PM2_Supp
6	*NEB* (*NM_001164508.2*)	chr2:152581466	c.412C > T (p. Arg138Ter)	EX7	Nonsense (Het)	LP	PVS1+PM2_Supporting
		chr2:152490436	c.9146T > G (p. Ile3049Ser)	EX65	Missense (Het)	VUS	PP3 + PM3+ PM2_Supporting
7	*TPM3* (*NM_152263.4*)	chr1:154145448	c.502C > T (p. Arg168Cys)	EX5	Missense (Het)	P	PS4 + PS2+PM1+ PM2_Supporting
8	*ACTA1* (*NM_001100.3*)	chr1:229568357	c.400A > G (p. Met134Val)	EX3	Missense (Het)	LP	PS2_Moderate+PP2 + PM5+ PM2_Supporting
9	*NEB* (*NM_001164508.2*)	chr2:152389953	c.21417 + 3A > G (p.?)	IVS144	Splicing (Hom)	P	PM4+PM3_Very Strong+PM2_Supp

EX*: exon*, IVS*: intron*, p.: protein, Het: Heterozygous, Hom: Homozygous, P: pathogenic, LP: Likely pathogenic, VUS: uncertain significance

Table 2
Salient features of our patient cohort with NM

Patient info									
No.	**1**	**2**	**3**	**4**	**5**	**6**	**7**	**8**	**9**
Age at onset	9 M	1 Y	9 M	2 Y	14 Y	4 Y	8 M	9 M	25^{+5}W
Age at diagnosis	9 M	1 Y	9 M	2 Y	14 Y	4 Y	8 M	9 M	25^{+5}W
Sex	F	M	M	M	M	F	F	M	N
Consanguinity	No	No	No	No	No	No	No	No	No
Gene	*NEB*	*NEB*	*NEB*	*NEB*	*NEB*	*NEB*	*TPM3*	*ACTA1*	*NEB*
Clinical features and LE(Unit): reference value									
Clinical features	DD, CHD	GDD, RP	Abnormal myocardial enzyme indicators, CH	RB	DD, Scoliosis, and Special Facial Features	RB	DD, Hypotonia	CHD, RP	CCH and FSE
Alanine transaminase (U/L): 7–30	-	21	-	27.4	-	15.3	21.5	109.7	-
Aspartate transaminase (U/L): 5–40	-	59.4	37.4	49.7	-	26.5	42.9	99.9	-
Lactate dehydrogenase (U/L): 114–240	-	424	323	564	-	304	-	670	-
Creatine Kinase (U/L): 0-190	-	30	214	47	-	140	-	48	-
Creatine Kinase isoenzyme (U/L): 0–25	-	24.7	45	64.1	-	56.2	-	65.3	-
α-hydroxybutyrate dehydrogenase (U/L): 72–182	-	331	258	412	-	221	-	623	-
Uric acid (umol/L): 155–357	-	140	-	248	-	356	-	99	-
Gesell Developmental Schedules (GDS)-DQ	-	-	-	-	-	-	59.2	-	-

Table 3
The following abbreviations are used in this manuscript

No.	Full name	Abbreviations
1	American College of Medical Genetics	ACMG
2	Cervical cystic hygroma	CCH
3	Congenital hypothyroidism	CH
4	Congenital heart disease	CHD
5	Computed Tomography	CT
6	Delayed motor development	DD
7	Fetal skin edema	FSE
8	Growth and developmental delay	GDD
9	Gesell Developmental Schedules	GDS
10	Human Gene Mutation Database	HGMD
11	Laboratory examination	LE
12	Nemaline myopathy-2	NEM2
13	Nemaline myopathy	NM
14	Patent foramen ovale	PFO
15	real-time quantitative polymerase chain reaction	qPCR
16	Relapsing bronchopneumonia	RB
17	Relapsing pneumonia	RP
18	Ultrasonic cardiogram	UCG
19	Ventricular septal defect	VSD
20	Whole-exome sequencing	WES
21	Normal Mode Analysis	NMA
22	Efficient Elastic Network Model	ENM

"-" indicates no laboratory examination, M male, F female, CHD congenital heart disease, DD delayed motor development, GDD growth and developmental delay, RP relapsing pneumonia, RB relapsing bronchopneumonia, CH congenital hypothyroidism, CCH cervical cystic hygroma, FSE fetal skin edema, LE laboratory examination.

4. Discussion

NM is a congenital, hereditary myopathy characterized by a complex and highly heterogeneous clinical phenotype, which is likely closely associated with mutations in multiple genes. To date, more than 12 genes have been implicated[19]. NM is defined by two key clinical diagnostic criteria: 1. Identification of characteristic nemaline rods (1–7 μm in length, 0.3-3.0 μm in width, appearing reddish-purple following modified Gomori trichrome staining) via muscle biopsy. 2. Detection of pathogenic variants in associated genes[20, 21]. For cases where biopsy or genetic evidence has not yet been obtained, a diagnosis may be established based on a comprehensive assessment of typical clinical features—primarily including proximal muscle weakness, hypotonia, and respiratory or swallowing difficulties—and/or normal to mildly elevated serum creatine kinase (CK) levels, as well as electromyography (EMG) findings suggestive of myopathic damage[20, 21]. In the small cohort examined in this study, muscle biopsies were unfortunately not performed on several patients due to the difficulty in obtaining tissue samples, however, whole-exome sequencing (WES) proved to be a valuable diagnostic tool for NM in these cases. Further studies have revealed substantial variability in symptom severity, with the clinical spectrum ranging from perinatal lethality and hypotonia to mild, non-progressive muscle weakness[21–23]. The age of onset also varies considerably, adding complexity to the diagnosis and management of this disease[24]. In the present study, we primarily identified pathogenic variants in the *NEB*, *ACTA1*, and *TPM3* genes, which findings consistent with those of previous studies. Notably, mutations in the *NEB* gene remain the most common cause of NM, accounting for ap-proximately 50% of all cases, followed by mutations in *ACTA1* and *TPM3*. The clinical phenotypes observed in our study cohort—including recurrent pneumonia, developmental delay, and severe non-progressive muscle weakness—align with reports from earlier studies, thereby highlighting the shared clinical characteristics of NM across diverse populations[25, 26]. Fortuitously, this study identified several unique phenotypes, such as the cystic hygroma and fetal skin edema observed in Patient 9, that are reported here for the first time. This not only highlights the clinical heterogeneity of the disease but also underscores the necessity of further in-depth exploration into the correlations between genotype and phenotype.

Investigating patients with NM presents complexities stemming not only from the high clinical and genetic heterogeneity of the disease but also from the unique structural features of the *NEB* gene—characteristics that significantly impede genetic analysis. The *NEB* gene is particularly notable for its extreme

complexity and substantial molecular weight, and it comprises 183 exons and spans a genomic sequence of 249 kb. The full-length transcript of this gene measures approximately 26 kb and encodes a protein with a molecular weight of approximately 800 kDa. The *NEB* gene encodes nebulin, a protein that extends along the entire length of the thin filament, with its C-terminus firmly anchored within the Z-disk structure and its N-terminus oriented toward the pointed end of the filament[27]. Consequently, employing traditional sequencing methods to investigate genomic variations proves to be both time-consuming and costly, often necessitating the expenditure of substantial time and resources. To overcome these challenges, we utilized NGS technology currently widely used in clinical practice, combined with bioinformatics tools, to conduct an in-depth analysis of the *NEB* gene[28]. Among the nine Chinese patients analyzed in this study, the vast majority presented with LOF variants within the *NEB* gene. Specifically, frameshift, nonsense, and splice variants—as well as the specific locations of these mutations—may serve as key pathogenic factors contributing to the observed phenotypic variability among individuals. However, missense variant may be the reason for relatively mild symptoms, or it may lead to the manifestation of other clinical features.

In this cohort of 9 patients diagnosed with NM, the splicing variant c.21417 + 3A > G was identified in three unrelated probands, corresponding to a detection rate of 33.3%. Of note, this variant has also been recurrently documented in independent Chinese NEM2 cohorts by Yin X et al. and Haidong L et al., with a relatively high prevalence observed among Chinese individuals[15, 29]. Combined with previous published evidence, our single-center data indicate that c.21417 + 3A > G is likely a hotspot variant for NEM2 in the Chinese population, which may be attributable to a potential founder effect in the Han Chinese population. Considering the relatively small sample size of the present study, further multi-center investigations with larger cohorts are warranted to validate its population enrichment and explore its correlation with clinical phenotypic spectra.

Apart from *NEB* gene mutations, the pathogenic variants in the *ACTA1* and *TPM3* genes also were more commonly the causes of NM, a finding that is consistent with previous research. Here, we describe two patients with NM associated with dominant *ACTA1* and *TPM3* mutations, respectively [30, 31]. To date, more than 250 *ACTA1* pathogenic mutations have been reported in the Human Gene Mutation Database (HGMD) (https://www.hgmd.cf.ac.uk/ac/index.php), missense mutations are the most frequently encountered type (accounting for 90%), but nonsense mutations (2.8%), splice mutations (2.8%), frameshift mutations (3.2%), as well as inframe and regulatory mutations have also been identified and recorded[32]. Those variants give rise to a spectrum of muscle disorders that are collectively categorized as actinopathies, and these disorders vary in terms of disease severity and the presence of histopathological hallmarks on muscle biopsy specimens. The range of manifestations is wide, with some actinopathies presenting with mild symptoms and subtle histological changes, while others cause severe muscle dysfunction and distinct pathological features observable under microscopic examination of muscle biopsy samples[33]. The variations in dis-ease severity and the specific histopathological hallmarks play a crucial role in accurately diagnosing and understanding the underlying mechanisms of these muscle dis-orders.

Similarly, mutations in *TPM3*, which encodes tropomyosin 3, are relatively rare but contribute to a distinct subset of NM cases. Nemaline myopathy type 1 (NEM1), caused by *TPM3* mutations, accounts for less than 5% of NM cases. Despite its rarity, *TPM3* mutations are of particular interest due to their role in regulating actin-myosin interactions and their potential impact on muscle fiber stability. The identification of *TPM3* mutations in our cohort underscores the importance of considering this gene in genetic testing panels for NM, particularly in cases with atypical clinical or histopathological features[34, 35].

The findings of this study serve as a crucial theoretical basis for the clinical diagnosis and treatment of patients, as well as for future research. First, the identification of pathogenic variants in patient associated genes, and their correlation with clinical phenotypes, underscores the necessity of whole-exome sequencing for patients with NM[36]. The application of NGS technology, combined with bioinformatics tools, provides robust evidence for identifying pathogenic variants and elucidating the correlations between genotype and phenotype[37]. This approach may offer guidance for formulating personalized treatment strategies for affected patients. Second, the identification of pathogenic fetal gene variants within our study cohort highlights the critical importance of early diagnosis. Early diagnosis of NM facilitates the timely implementation of interventions, which may ultimately enhance patients' quality of life[38–40]. Furthermore, follow-up studies are warranted to gain a deeper understanding of the natural history of NM and to identify factors that influence disease progression. Finally, the findings of this study lay the groundwork for future in-depth investigations into the underlying molecular mechanisms of NM. Con-ducting functional studies on the identified variants—particularly those involving the *NEB*, *ACTA1*, and *TPM3* gene—is essential for understanding how these mutations disrupt muscle function and drive disease pathogenesis; such studies hold promise for providing a foundation for the development of targeted therapies, such as gene re-placement therapy, RNA-based therapies, or small-molecule inhibitors[41–43].

5. Conclusion

In summary, this study utilized NGS technology to diagnose 9 patients with NM, which including 8 postnatal patients and 1 prenatal fetus, and combine with relevant bioinformatics analyses, preliminarily explored and elucidated the genetic and clinical heterogeneity of NM. We focused on analyzing and reviewing mutations within the *NEB* gene, conducting an in-depth analysis of the specific variant sites identified in this study, and for partial LOF variants, we employed AlphaFold3 to predict the structure of the encoded protein, while for missense mutations were utilized NMA to assess their thermodynamic effects, thereby preliminarily revealing the pathogenic mechanisms underlying *NEB* gene missense variants. Our study not only expands the spectrum of genetic mutations and phenotypes associated with NM but also provides a theoretical basis for developing personalized management strategies for patients with this condition. However, this study is subject to several limitations. First, we were able to obtain only limited clinical visit records for the patients and lacked access to their complete medical histories. Second, while we conducted an exploratory analysis of the *NEB* gene using NMA, we were unable to validate these findings due to the limited number of cases available, and future studies should aim to collect a larger cohort of cases to validate these results and substantiate the predictive utility of NMA for *NEB* gene missense variants. Finally, owing to the difficulties associated with sample acquisition, muscle biopsies were not performed to provide corroborating evidence. Future research should focus on further elucidating the molecular mechanisms underlying the pathogenesis of NM and developing targeted therapeutic interventions to improve the prognosis for affected individuals. By deepening our understanding of the genetic architecture and pathophysiology of NM, we hope to take a solid step forward on the path toward achieving precision medicine for this challenging disease.

Declarations

Informed Consent Statement

All participants provided written informed consent prior to enrollment in this study, all clinical specimens and related data were used only for academic research purposes. This study was conducted in accordance with the Declaration of Helsinki and approved by the local ethics committee.

Conflicts of Interest

The authors declare no conflicts of interest.

Funding

This research was funded by the National Natural Science Foundation of China (Grant No. 82560331) and the Hospital Research Fund Project (Grant No. GMCCH2025-2-3-05).

Author Contribution

B.Z.: Conceptualization, Methodology, Visualization, Writing-original draft; C.Z., L.Z.and Y.B.: Investigation, Writing review & editing; X.L, P.M. and Y.W.: Validation; S.H., L.H. and Y.B.: Supervision, Project administration, Funding acquisition. All authors reviewed the manuscript.

Acknowledgement

We sincerely thank all participants for their participation and cooperation in this study. We also appreciate the support from our hospital and department. Special thanks go to all colleagues who provided valuable suggestions and technical assistance during the research.

Data Availability

We fully understand and agree that sharing raw data is crucial for the reproducibility of academic research. However, in accordance with our medical ethics review guidelines and the informed consent signed by all participants, the complete raw dataset cannot be publicly uploaded to journal databases to strictly protect patient privacy and avoid the risk of personal information leakage. To balance data transparency and patient privacy, we have prepared de-identified and anonymized data that does not contain any identifiable personal information and submitted it to BioProject under the number PRJNA1494031 (https://www.ncbi.nlm.nih.gov/bioproject/PRJNA1494031).

References

1. Sewry, C. A., Laitila, J. M. & Wallgren-Pettersson, C. Nemaline myopathies: a current view. *J. Muscle Res. Cell. Motil.* **40**, 111–126. 10.1007/s10974-019-09519-9 (2019).
2. Lehtokari, V. L. et al. Self-reported functioning among patients with ultra-rare nemaline myopathy or a related disorder in Finland: a pilot study. *Orphanet J. Rare Dis.* **18**, 374. 10.1186/s13023-023-02973-2 (2023).
3. Robaszkiewicz, K. et al. A Novel Variant in TPM3 Causing Muscle Weakness and Concomitant Hypercontractile Phenotype. *Int. J. Mol. Sci.* **24** 10.3390/ijms242216147 (2023).
4. Wang, Q. et al. Mutational and clinical spectrum in a cohort of Chinese patients with hereditary nemaline myopathy. *Clin. Genet.* **97**, 878–889. 10.1111/cge.13745 (2020).
5. Gartz, M. et al. ACTA1 H40Y mutant iPSC-derived skeletal myocytes display mitochondrial defects in an in vitro model of nemaline myopathy. *Exp. Cell. Res.* **424**, 113507. 10.1016/j.yexcr.2023.113507 (2023).
6. McAdow, J. et al. A pathogenic mechanism associated with myopathies and structural birth defects involves TPM2-directed myogenesis. *JCI Insight*. **7** 10.1172/jci.insight.152466 (2022).
7. Yavas, C. et al. A rare TNNT1 gene variant causing creatine kinase elevation in nemaline myopathy: c.271_273del (p.Lys91del). *Genes Genomics*. **46**, 613–620. 10.1007/s13258-024-01502-0 (2024).
8. de Winter, J. M. et al. KBTBD13 is an actin-binding protein that modulates muscle kinetics. *J. Clin. Invest.* **130**, 754–767. 10.1172/JCI124000 (2020).
9. Rosen, S. M. et al. Knockin mouse model of the human CFL2 p.A35T mutation results in a unique splicing defect and severe myopathy phenotype. *Hum. Mol. Genet.* **29**, 1996–2003. 10.1093/hmg/ddaa035 (2020).
10. Buchignani, B. et al. KLHL40-Related Myopathy: A Systematic Review and Insight into a Follow-up Biomarker via a New Case Report. *Genes (Basel)*. **15** 10.3390/genes15020208 (2024).

11. Jirka, C. et al. Dysregulation of NRAP degradation by KLHL41 contributes to pathophysiology in nemaline myopathy. *Hum. Mol. Genet.* **28**, 2549–2560. 10.1093/hmg/ddz078 (2019).
12. Schatz, U. A. et al. Evidence of mild founder LMOD3 mutations causing nemaline myopathy 10 in Germany and Austria. *Neurology* ;91:e1690-e1694. (2018). 10.1212/WNL.0000000000006428
13. Merlini, L. et al. Congenital myopathy with hanging big toe due to homozygous myopalladin (MYPN) mutation. *Skelet. Muscle*. **9**, 14. 10.1186/s13395-019-0199-9 (2019).
14. Calame, D. G. et al. Biallelic Pathogenic Variants in TNNT3 Associated With Congenital Myopathy. *Neurol. Genet.* **7**, e589. 10.1212/NXG.0000000000000589 (2021).
15. Yin, X. et al. Clinico-pathological features and mutational spectrum of 16 nemaline myopathy patients from a Chinese neuromuscular center. *Acta Neurol. Belg.* **122**, 631–639. 10.1007/s13760-020-01542-9 (2022).
16. Gajda, A. et al. Nemaline myopathy type 2 (NEM2): two novel mutations in the nebulin (NEB) gene. *J. Child. Neurol.* **30**, 627–630. 10.1177/0883073813494476 (2015).
17. Skjærven, L. et al. Integrating protein structural dynamics and evolutionary analysis with Bio3D. *BMC Bioinform.* **15**, 399. 10.1186/s12859-014-0399-6 (2014).
18. Rodrigues, C. H. M., Pires, D. E. V. & Ascher, D. B. DynaMut2: Assessing changes in stability and flexibility upon single and multiple point missense mutations. *Protein Sci.* **30**, 60–69. 10.1002/pro.3942 (2021).
19. Gurgel-Giannetti, J. et al. Nemaline Myopathy in Brazilian Patients: Molecular and Clinical Characterization. *Int. J. Mol. Sci.* **23** 10.3390/ijms231911995 (2022).
20. Wang, Y. et al. Muscle MRI Changes in Nebulin-Related Nemaline Myopathy. *Muscle Nerve*. **72**, 580–585. 10.1002/mus.28465 (2025).
21. Laitila, J. & Wallgren-Pettersson, C. Recent advances in nemaline myopathy. *Neuromuscul. Disord*. **31**, 955–967. 10.1016/j.nmd.2021.07.012 (2021).
22. Malfatti, E. & Romero, N. B. Nemaline myopathies: State of the art. *Rev. Neurol. (Paris)*. **172**, 614–619. 10.1016/j.neurol.2016.08.004 (2016).
23. Lehtokari, V. L. et al. Mutation update: the spectra of nebulin variants and associated myopathies. *Hum. Mutat.* **35**, 1418–1426. 10.1002/humu.22693 (2014).
24. Bojdo, A. et al. [Nemaline myopathy as a cause of neonatal hypotonia - with emphasis on personal experiences. Report of a family with two brothers affected]. *Med. Wieku Rozwoj*. **13**, 5–10 (2009).
25. Zheng, W. et al. [Genetic analysis of a patient with Rod-shaped myopathy due to variants of NEB gene]. *Zhonghua Yi Xue Yi Chuan Xue Za Zhi*. **41**, 1473–1477. 10.3760/cma.j.cn511374-20240620-00343 (2024).
26. Schroder, J. M., Durling, H. & Laing, N. Actin myopathy with nemaline bodies, intranuclear rods, and a heterozygous mutation in ACTA1 (Asp154Asn). *Acta Neuropathol.* **108**, 250–256. 10.1007/s00401-004-0888-1 (2004).
27. Karimi, E. et al. Characterization of NEB pathogenic variants in patients reveals novel nemaline myopathy disease mechanisms and omecamtiv mecarbil force effects. *Acta Neuropathol.* **147**, 72. 10.1007/s00401-024-02726-w (2024).
28. Lee, J. M. et al. Clinical and genetic diversity of nemaline myopathy from a single neuromuscular center in Korea. *J. Neurol. Sci.* **383**, 61–68. 10.1016/j.jns.2017.10.020 (2017).
29. Haidong, L. et al. Clinico-pathological and gene features of 15 nemaline myopathy patients from a single Chinese neuromuscular center. *Acta Neurol. Belg.* **124**, 91–99. 10.1007/s13760-023-02333-8 (2024).
30. Moreno, C. A. M. et al. Clinical and Histologic Findings in ACTA1-Related Nemaline Myopathy: Case Series and Review of the Literature. *Pediatr. Neurol.* **75**, 11–16. 10.1016/j.pediatrneurol.2017.04.002 (2017).
31. Bevilacqua, J. A. et al. Novel autosomal dominant TPM3 mutation causes a combined congenital fibre type disproportion-cap disease histological pattern. *Neuromuscul. Disord*. **32**, 687–691. 10.1016/j.nmd.2022.05.014 (2022).
32. Stenson, P. D. et al. The Human Gene Mutation Database: towards a comprehensive repository of inherited mutation data for medical research, genetic diagnosis and next-generation sequencing studies. *Hum. Genet.* **136**, 665–677. 10.1007/s00439-017-1779-6 (2017).
33. Martinez-Diago, C. et al. Novel variant in ACTA1 identified in a fetus with akinesia deformation sequence and cortical development delay. *Prenat Diagn.* **44**, 996–998. 10.1002/pd.6568 (2024).
34. Laing, N. G. et al. A mutation in the alpha tropomyosin gene TPM3 associated with autosomal dominant nemaline myopathy. *Nat. Genet.* **9**, 75–79. 10.1038/ng0195-75 (1995).
35. Pelin, K. et al. Mutations in the nebulin gene associated with autosomal recessive nemaline myopathy. *Proc. Natl. Acad. Sci. U S A*. **96**, 2305–2310. 10.1073/pnas.96.5.2305 (1999).
36. de Feraudy, Y. et al. Exome sequencing in undiagnosed congenital myopathy reveals new genes and refines genes-phenotypes correlations. *Genome Med.* **16**, 87. 10.1186/s13073-024-01353-0 (2024).
37. Schnitzler, L. J. et al. Sporadic late-onset nemaline myopathy: clinico-pathological characteristics and review of 76 cases. *Orphanet J. Rare Dis.* **12**, 86. 10.1186/s13023-017-0640-2 (2017).
38. Lehtokari, V. L. et al. Nutritional status of patients with nemaline myopathy and related congenital myopathies in Finland: A pilot study. *J. Neuromuscul. Dis.* **12**, 22143602241303374. 10.1177/22143602241303374 (2025).
39. Fabian, L. et al. Comprehensive phenotypic characterization of an allelic series of zebrafish models of NEB-related nemaline myopathy. *Hum. Mol. Genet.* **33**, 1036–1054. 10.1093/hmg/ddae033 (2024).

40. Fox, M. D. et al. TNNT1 nemaline myopathy: natural history and therapeutic frontier. *Hum. Mol. Genet.* **27**, 3272–3282. 10.1093/hmg/ddy233 (2018).
41. Fisher, G. et al. Early clinical and pre-clinical therapy development in Nemaline myopathy. *Expert Opin. Ther. Targets*. **26**, 853–867. 10.1080/14728222.2022.2157258 (2022).
42. de Winter, J. M. et al. Effect of levosimendan on the contractility of muscle fibers from nemaline myopathy patients with mutations in the nebulin gene. *Skelet. Muscle*. **5**, 12. 10.1186/s13395-015-0037-7 (2015).
43. Farkas, D. et al. Peripheral thickening of the sarcomeres and pointed end elongation of the thin filaments are both promoted by SALS and its formin interaction partners. *PLoS Genet.* **20**, e1011117. 10.1371/journal.pgen.1011117 (2024).

Figures

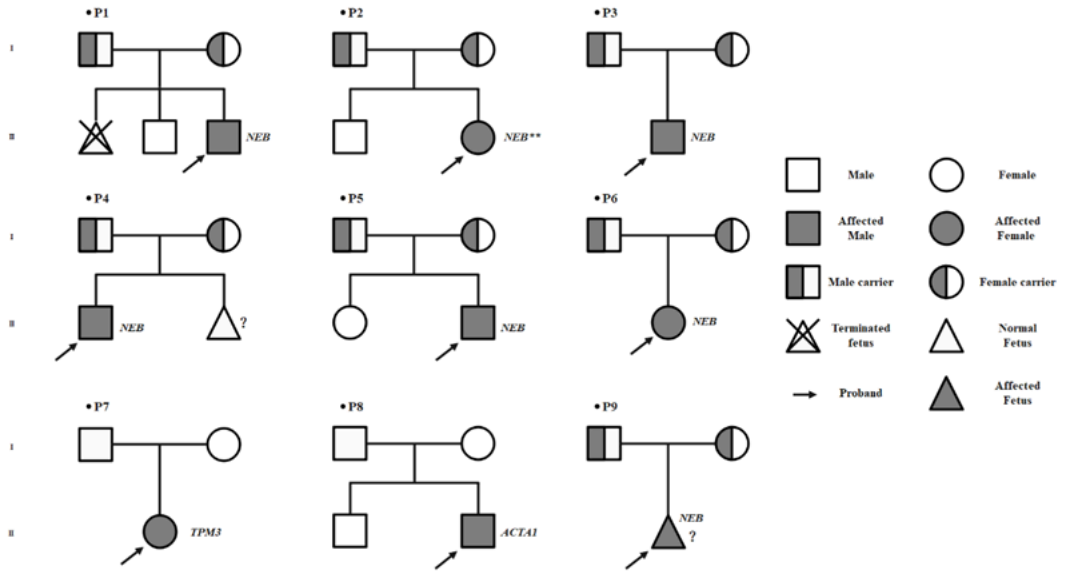


Figure 1

The pedigree chart of these nine patients with NM. **Indicates that four allelic variants were found in the NEB gene in this family.

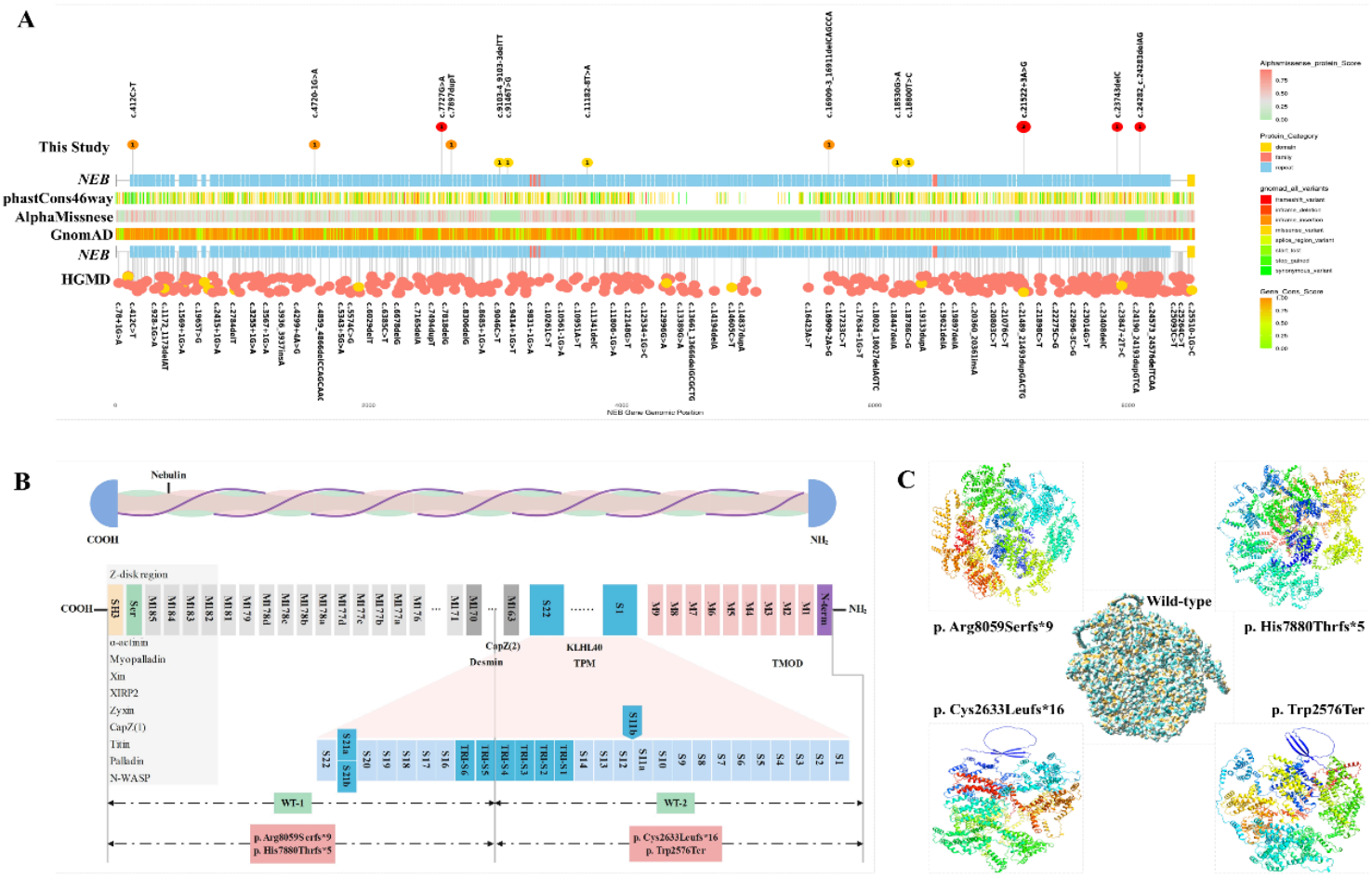


Figure 2

Collected and analyze *NEB*gene reported variants and shown the structure of the Nebulin protein and its binding partners, aiming to deepen the understanding of the *NEB* gene and its corresponding Nebulin protein. A. The middle part of the two protein modules, when observed from the top to the bottom, is composed of the human *NEB*gene conservation score, the Alphamissnese prediction score of *NEB* gene missense variants, and the *NEB* gene variant frequency of the gnomAD database. It is quite evident and unmistakable that these pathogenic variants tend to occur in regions that possess a higher degree of conservation. B. The Structure of the actin binding protein Nebulin and its binding partners. The Nebulin gene consists of multiple repetitive modules (M), which contain actin-binding domains (S1–S22 super-repeat sequences). These super-repeat sequences encode mutually exclusive splice variants—exons 143 and 144—and harbor the binding site for *KLHL40*. The C-terminus anchors to the Z-disc region of the sarcomere and contains a conserved, serine rich homology domain (SH3). The amino acid sequences selected for the predicted protein structure are highlighted based on the presence or absence of these super-repeat sequences. C. We utilized AlphaFold3 to predict and construct a three-dimensional model of the Nebulin protein, thereby enabling the visualization of the spatial structure of the LoF variant protein.

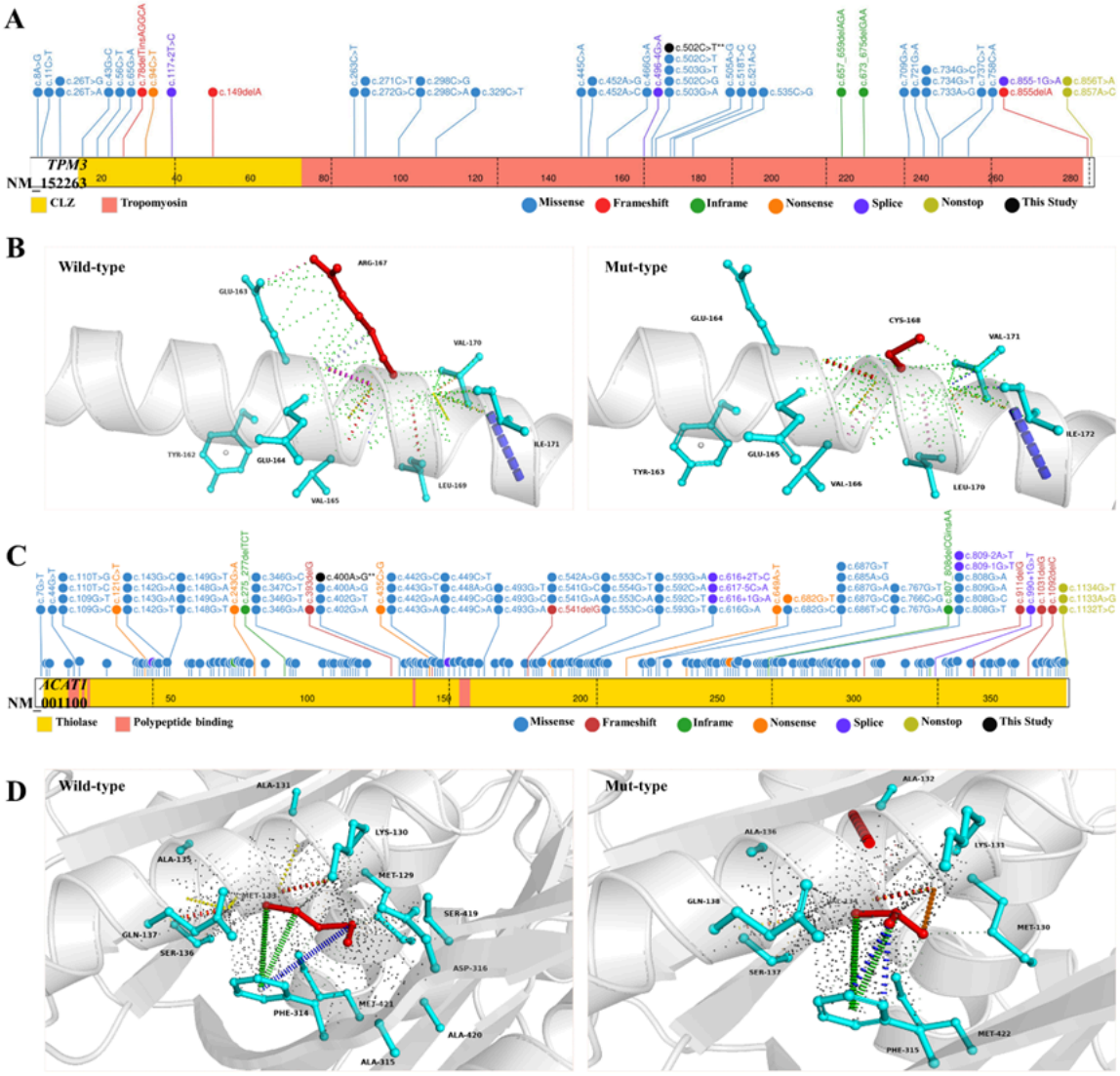


Figure 3

Display the reported variants information of *TPM3* and *ACTA1* genes in HGMD database. A. Shown the reported variants information of *TPM3* in HGMD database, the distinct colors represent different variant types. B. Dynamut2 predicts the changes in the intermolecular forces between the tropomyosin alpha3 chain proteins before and after mutation to reflect the stability and flexibility of proteins after mutation. C. Shown the reported variants information of *ACTA1* in HGMD database. D. Dynamut2 predicts the changes in the intermolecular forces between actin proteins before and after mutation to reflect the stability and flexibility of proteins after mutation.

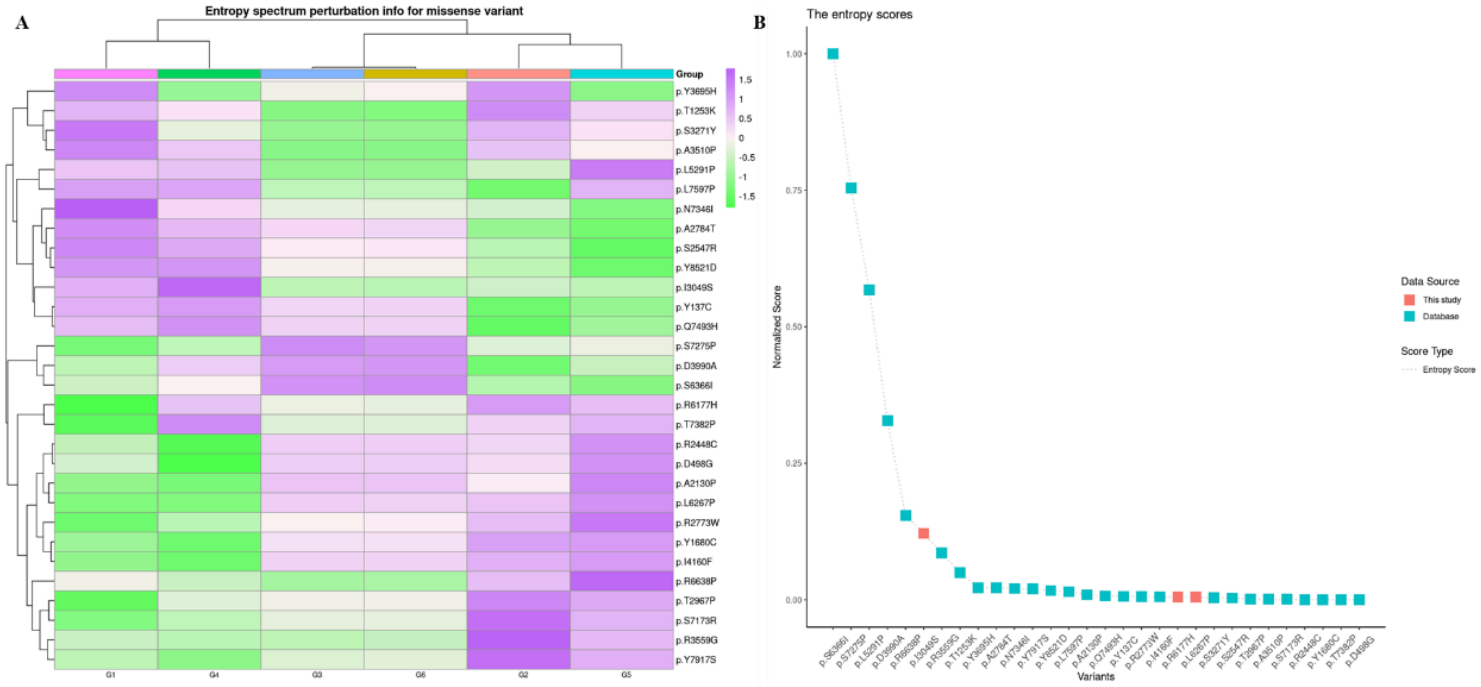


Figure 4

Thermodynamic Profiles of the *NEB*Gene Variants. A. Shown the heatmap for thermo-dynamic analysis of proteins the vertical axis depicts the various variables derived from the analysis of each variant. The color scale denotes the normalized z-score. B. Shown the combined normalized scores, represented by the formula (S1*S4 + S2*S5 + S3*S6), were used to describe the entropy of variants. The differences in these entropy scores are then presented to illustrate the harmful properties of proteins.

Supplementary Files

This is a list of supplementary files associated with this preprint. Click to download.

- Supplementarymaterial.pdf